Distributed generation (DG) is revolutionizing contemporary power systems by integrating decentralized power sources into the grid. One critical challenge in DG deployment is ensuring stable voltage levels, given the intermittent nature of renewable energy sources and varying loads. This work examines voltage correction techniques in DG systems, focusing on the role of power electronics in maintaining grid stability. Through advanced control algorithms and real-time monitoring, power electronic devices such as inverters enable precise voltage regulation, reactive power compensation, and mitigation of voltage fluctuations. Various strategies for voltage correction, including reactive power injection, voltage regulation, and harmonic filtering, are explored, highlighting their effectiveness in enhancing power quality and system reliability.

Dr. P. Marimuthu , Professor, EEE Department, **Malla Reddy Engineering Colleg**e, Secunderabad, Telangana, India.
Dr. Moorthy Veerasamy, Professor in School of Engineering & Controller of Examinations, **Mohan Babu University**, Tirupati, Andhra Pradesh, India.

9 7 8 6 2 0 7 4 6 2 1 9 3

P. Marimuthu
Moorthy Veerasamy

Voltage Correction in Distributed Generation

LAP LAMBERT Academic Publishing

P. Marimuthu
Moorthy Veerasamy

Voltage Correction in Distributed Generation

P. Marimuthu
Moorthy Veerasamy

Voltage Correction in Distributed Generation

LAP LAMBERT Academic Publishing

Imprint
Any brand names and product names mentioned in this book are subject to trademark, brand or patent protection and are trademarks or registered trademarks of their respective holders. The use of brand names, product names, common names, trade names, product descriptions etc. even without a particular marking in this work is in no way to be construed to mean that such names may be regarded as unrestricted in respect of trademark and brand protection legislation and could thus be used by anyone.

Cover image: www.ingimage.com

Publisher:
LAP LAMBERT Academic Publishing
is a trademark of
Dodo Books Indian Ocean Ltd. and OmniScriptum S.R.L publishing group

120 High Road, East Finchley, London, N2 9ED, United Kingdom
Str. Armeneasca 28/1, office 1, Chisinau MD-2012, Republic of Moldova, Europe
Printed at: see last page
ISBN: 978-620-7-46219-3

Contents

Chapter 1

Introduction

1.1 Motivation of study

There is an agreement between most researchers that the use of fossil fuels has to be reduced compared to the situation today. The Kyoto Protocol requires developed countries to reduce their greenhouse gas emissions below levels specified for each of them. These targets must be met within a five-year time frame between 2008 and 2012, and add up to a total cut in emissions of at least 5 percent against the baseline of 1990.[2] The Treaty became operative 16 February 2005 and Norway signed not to increase the greenhouse gas emissions with more than one percent compared to the 1990 level. In 2005 Norway had increased the emissions by 8 percent compared to the 1990 level.[3]

Environmental protection, energy saving and improved energy efficiency are important topics to fulfil the aims of the Kyoto protocol. However the demand for electricity continues to grow. 40% of all energy consumption today is in electrical energy and this is expected to grow to 60% by 2040[4]. The invention of power electronics have enabled possibilities to decrease energy consumption with more efficient energy systems.

The main task in this thesis is to make a simulation program of a small ac distribution system with a Constant Power Load (CPL) consisting of a power electronic converter. Background study and theory of simulation model will be presented. To verify that the load act as CPL a simulation study will be done to delineate the typical behaviour of a CPL. Simulations will be carried out to compare a passive CPL with no reactive compensation with an active CPL which inject reactive power into the system. The comparison regard voltage support. Some considerations on advantages and disadvantages with the reactive control will be discussed.

1.2 Power electronics in AC distribution systems

The use of power electronics in distributed power systems is increasing in the areas of generation interface, energy storage and loads. It is predicted that the share of electrical energy which will be controlled by power electronics will increase from 40% in 2000 to 80% in 2015[4]. Hence power electronics will have a considerable responsibility for the reliability and stability of future power systems. Expansion of renewable energy in power systems call for more use of power electronics for efficient control and grid integration.

The progress in power electronics has been possible primarily due to improvement of power semiconductor devices[5]. Development in converter topologies, pulse-width-modulation (PWM) techniques, control and estimation techniques, analytical and simulation methods, computers, digital signal processors, control hardware and software, etc. have also contributed to the improvement in power electronics. The invention of the thyristor started the modern era of solid state power electronics. After this invention a series of transistors and thyristors have been developed. In the system under study a converter consisting of 6 insulated gate bipolar transistors (IGBTs) with power diodes in anti-parallel will be studied. The converter uses a matrix of power semiconductor switches to convert electrical power at high efficiency. Presently available IGBT converters for distribution use are rated at 1-2 MVA but can be connected in parallel to give overall system ratings of up to 10 MVA[6].

A distribution system with high percentage of power electronic loads may be unstable under abnormal operating conditions like voltage sag or a phase to ground fault. Since voltage source converters have the ability to produce and absorb reactive power, this study will investigate a voltage source converter for voltage support in a distributed power system. Regulated converters with high bandwidth control systems in the power electric loads can act as constant power loads. This type of load is the main component in the research in this thesis. Simulation results shows how the converter regulator design affects the voltage in the system.

Chapter 2

Background

2.1 Electrical power grid in Norway

There are three levels in the Norwegian electricity grid: main grid, regional grid and distribution grid[7]. The main grid is the spine of the transmission grid with voltages at 420, 300 and 132 kV. Statnett owns about 90 per cent of the main grid and manages this system. The voltage levels of the regional grid are often 132, 66 and 45 kV. At the lowest voltage levels the distribution grid transport current to different loads. The distribution grid divides into high voltage at 22- 11 kV and low voltage at 400- 230 V[8].

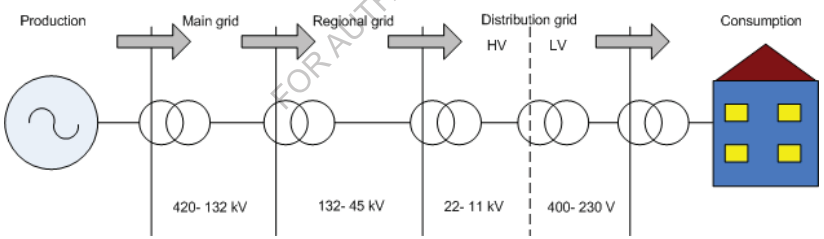

Figure 2.1: The Norwegian power grid.

2.2 Distributed AC system

In figure 2.1 it can look like the last part of the electricity grid only contains loads. However this is very often not the case. Distributed AC system is composed of both generation and various types of loads. It is generally desirable to have generation of electrical energy as close to consumption as possible. An illustration of a typical distribution system is depicted in

figure 2.2. The generation can for instance be wind farms or small hydro-electric power stations. If a power system has a lot of wind power generation it can result in poor power quality and poor stability margins. One method to improve power quality and stability margins can be to use a static compensator(STATCOM)[9]. Another method under investigation is to use power electronic controlled loads for voltage support[10]. It is this method that will be under investigation in this thesis.

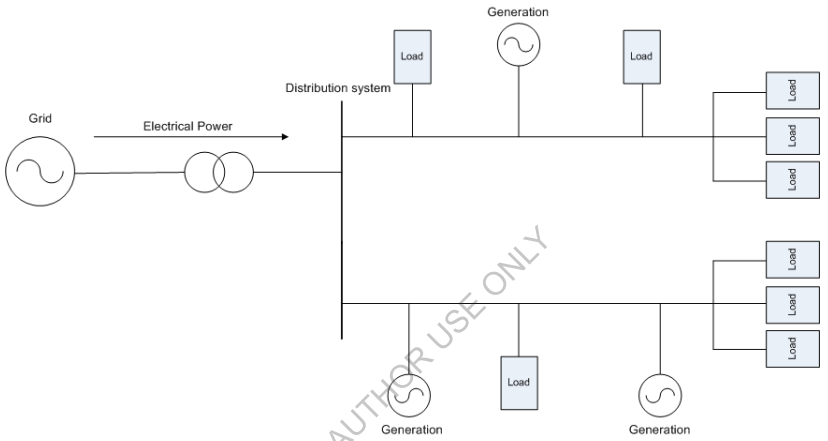

Figure 2.2: Example of a distributed AC system.

A distributed power system is characterized by distribution of the power processing functions among many power processing units(PPUs)[11]. One PPU is shown in figure 2.2 and a connection of three PPUs is shown in figure 2.3.

With the expansion of solid- state devices in AC power systems to improve the performance and flexibility, motor drives and power electronic converters are extensively used in loads[12]. This will be the focus of research in this thesis.

The loads in these systems can behave passive or active. Passive loads consume power from the system without regard to system stability. In contrast an active load is an active participant in regard to system stability. An example of the difference between these types of loads will be examined later through simulations.

Most loads in these systems require constant voltage and frequency. Static

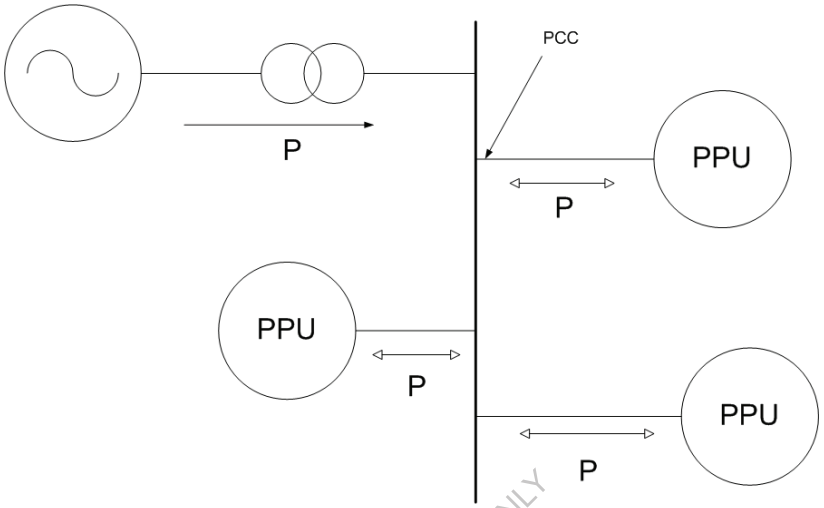

Figure 2.3: Three PPUs connected together in a distributed AC system. *PCC* denote point of common coupling. It is the point where the PPU connect to the common grid.

load models express active and reactive steady state powers as functions of the bus voltage at a given frequency. Loads in these systems are typically categorized as follows[13]:

- Constant impedance load model, where the power varies with a square of the voltage magnitude.
- Constant current load model, where the power varies directly with the voltage magnitude.
- Constant power load model, where the power does not vary with changes in voltage magnitude.

This work will involve the constant power load model.

2.3 Constant Power Load

The amount of constant power loads (CPLs) consisting of solid-state self-regulated power converters and inverters are increasing in many electrical

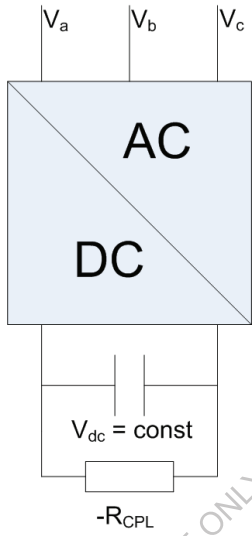

Figure 2.4: Constant power load.

power distribution systems[14]. When a power electronic converter is tightly regulated it can behave as a CPL. Such type of load draws constant active power from the system irrespective of system condition. It is capable of high bandwidth regulation and high power conversion efficiency. These qualities are desirable, but may also cause system instabilities and eventually failure of operation if not prevented. High bandwidth regulation combined with filtering elements in the system can result in negatively damped oscillations in the AC system. This is known as negative resistance behaviour.

A schematic drawing of one CPL is depict in figure 2.4. $-R_{cpl}$ demonstrate the negative resistance seen from the AC distribution system. This small-signal non-linear input resistance can be calculated from the fact that input power and output power are equal[15]. Equation 2.1 shows this relation. This equation is valid for frequencies below the switching frequency and for high bandwidth regulation of the converter[14]. Differentiating the voltage with respect to current gives the negative input resistance as derived in equation 2.2. The DC voltage is fixed and the amount of current drawn is dependent on the quantity of power required by the load.

$$\begin{aligned} P_{in} = P_{out} = v \cdot i \\ v = \frac{P}{i} \end{aligned} \tag{2.1}$$

$$\frac{dv}{di} = -i^{-2} \cdot P = -\frac{P}{i^2} = -\frac{v^2}{P} = -R_{cpl} \tag{2.2}$$

2.3.1 Negative resistance behaviour

Negative incremental resistance characteristic is typical for a constant power load. Decreasing fault resistance result in reduction of AC system voltage during a fault. As a consequence the operations of the internal controller make the converter draw more current from the system. This voltage oriented control of the converter is regulated to maintain the active power input to the converter at a constant value regardless of system condition. A voltage oriented vector control technique will be presented in the next chapter. The DC voltage and current are constant while there is a fault in the AC distribution system.

The static input voltage - current characteristic for the load is shown in figure 2.5. The plot is a hyperbola since P_{in} is a constant value. Figure 2.5 shows two different values of input resistance, $-R_{cpl1}$ and $-R_{cpl2}$, at two different converter operating points. This curve is known as negative resistance curve because the slope of this curve is negative. Verification of this curve will be done for the case under study in the following chapters.

With this drawback of the CPL in regard to system stability a method to reduce this effect is desirable. Injecting reactive current from the CPL is an alternative presented in this thesis.

2.4 Reactive Power Compensation

Reactive power compensation, or Var compensation, is defined as the management of reactive power to improve the performance of ac power systems[16]. Most power quality problems can be attenuated or solved with an adequate control of reactive power. Reactive power compensation is viewed from two aspects:

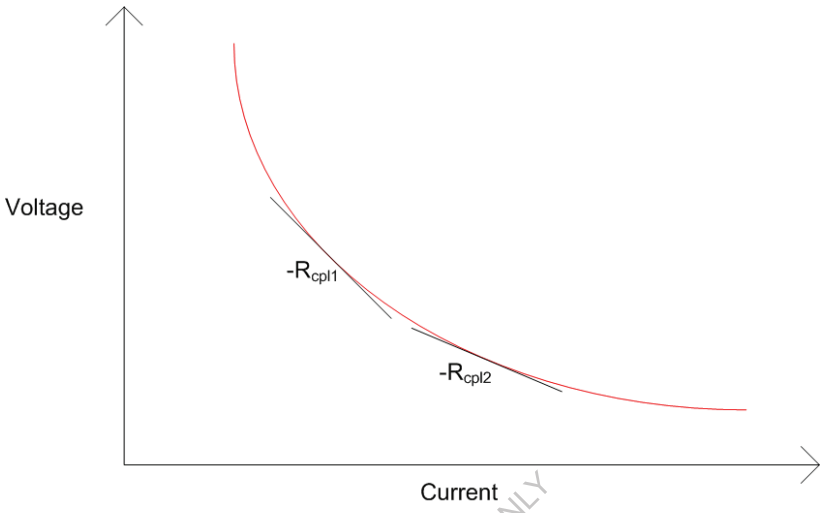

Figure 2.5: Negative resistance curve typical for CPLs.

- load compensation, for increasing the system power factor, to balance the real power drawn from the ac supply, to compensate voltage regulation, and to eliminate current harmonic components produced by large and fluctuating nonlinear industrial loads.
- voltage support, to reduce voltage fluctuation at a given terminal of a transmission line.

Var compensation in transmission systems also improves the stability of the ac system by increasing the maximum active power that can be transmitted and by keeping a substantially flat voltage profile throughout the ac system.

Rotating synchronous condensers and fixed or mechanically switched capacitors or inductors have been the traditional method for reactive power compensation. A synchronous condenser is simply a synchronous machine connected to the power system. In recent years static Var compensators (SVCs) employing thyristor-switched capacitors (TSCs) and thyristor-controlled reactors (TCRs) have been developed to provide and absorb required reactive power. Another method is the use of self-commutated pulse-width-modulation (PWM) converters that permits the implementation of static compensators capable of generating or absorbing reactive current components with a time response faster than the fundamental power network cycle.

Table 2.1 compares these four basic types of compensators[16].

In this work a PWM converter controlling a constant power load for reactive compensation will be investigated.

Reactive compensators				
	Synchronous Condenser	**TCR(with shunt capacitors if necessary)**	**TSC(with TCR if necessary)**	**Self-commutated Compensator**
Accuracy of compensation	Good	Very good	Good, very good with TCR	Excellent
Control flexibility	Good	Very good	Good, very good with TCR	Excellent
Reactive power capability	Leading or Lagging	Leading or Lagging indirect	Leading or Lagging indirect	Leading or Lagging
Control	Continuous	Continuous	Discontinuous (Cont. with TCR)	Continuous
Response time	Slow	Fast, 0.5 to 2 cycles	Fast, 0.5 to 2 cycles	Very fast, but dependent on the control system and switching frequency
Harmonics	Very good	Very high(large-size filters needed)	Good (filters are necessary with TCR)	Good, but dependent on switching pattern
Losses	Moderate	Good, but increase in lagging mode	Good, but increase in lagging mode	Very good, but increase with switching frequency
Phase balancing ability	Limited	Good	Limited	Very good with 1-ϕ unites, limited with 3-ϕ unites
Cost	High	Moderate	Moderate	Low to moderate

Table 2.1: Comparison of basic types of reactive power compensators.

Chapter 3

The System Under Study

3.1 The distributed AC system

The AC distribution system contains a distributed generation system modelled as an asynchronous machine, a distribution grid, two transformers with voltage levels at 690 V and 22 kV, a constant power load and electrical lines to connect the components together. The generation and the load operate at 690 V and connect to the distribution grid through two transformers. Figure 3.1 shows the system under study.

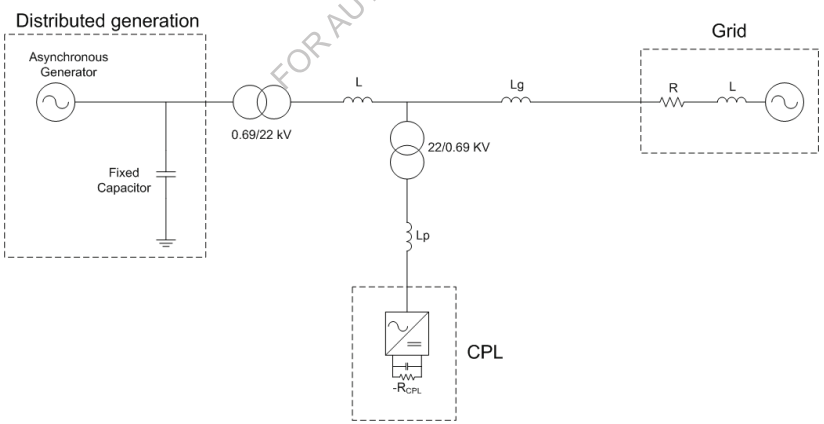

Figure 3.1: The system

The constant power load is a tightly regulated power electronic AC/DC converter that keeps the power drawn from the system to the load constant.

3.2 Base System for Per Unit Transformation

A per unit (PU) reference system makes it easy to determine the real value of a generic quantity by multiplying with the base value chosen. The pu-system gives a consistent system description that is not tied up to a particular component through this component's rated value. It it easy to compare powers, voltages, currents and impedances when a common reference system is calculated for the whole system. In the case of this thesis it is important to compare voltages and currents on the AC and DC side of the converter and therefore orderly with a global pu- system. The method for calculating the pu- system is frequently used in the electric drives field of research [17]-[18]. The following reference values are chosen:

$$\begin{aligned} S_b &= 800[kVA] \\ V_{b1} &= \sqrt{\frac{2}{3}} \cdot 690[V] = 563.38[V] \\ V_{b2} &= \sqrt{\frac{2}{3}} \cdot 22000[V] = 17962.92[V] \\ \omega_b &= 2 \cdot \pi \cdot f_n = 314.159[rad/s] \end{aligned} \tag{3.1}$$

where S_b is the base three-phase power of the ac-grid while V_{b1} and V_{b2} are the base peak phase voltages at the primary and secondary side of the transformer. f_n is the nominal generator frequency and ω_b is the base frequency in rad/s. Base current and impedance of the primary side are calculated as:

$$\begin{aligned} I_{b1} &= \frac{2}{3} \cdot \frac{S_b}{V_{b1}} = 946.66[A] \\ Z_{b1} &= \frac{V_{b1}}{I_{b1}} = 0.595[\Omega] \end{aligned} \tag{3.2}$$

while base values for current and impedance referred to secondary side are:

$$\begin{aligned} I_{b2} &= \frac{2}{3} \cdot \frac{S_b}{V_{b2}} = 29.69[A] \\ Z_{b2} &= \frac{V_{b2}}{I_{b2}} = 605[\Omega] \end{aligned} \tag{3.3}$$

To keep the control voltage of the PWM within the peak of the triangular waveform and prevent over-modulation, the DC side voltage should not be

less than two times the base voltage as shown in equation 3.4. The concept of over-modulation will be explained in section 3.7.5.

$$V_{dc} = 2 \cdot \sqrt{\frac{2}{3}} \cdot V_{LL,rms} = 2 \cdot V_{peak,ph} = 2 \cdot V_{b1} = 1126.77[V] \tag{3.4}$$

With the power balance in equation 3.5 it is possible to find the base current given in equation 3.6.

$$S_{3ph} = 3 \cdot V_{ph} \cdot I_{ph} = \frac{3}{2} \cdot V_{b1} \cdot I_{b1} = V_{dcbase} \cdot I_{dcbase} \tag{3.5}$$

$$I_{dcbase} = \frac{3}{4} \cdot I_b 1 = 710[A] \tag{3.6}$$

And base dc impedance is calculated from ohms law:

$$Z_{dcbase} = \frac{V_{dcbase}}{I_{dcbase}} = 1.587[\Omega] \tag{3.7}$$

3.3 Distributed generation

An asynchronous machine can work as a motor or a generator. It is termed motor when it converts electrical power to mechanical power, and generator for the opposite case. Asynchronous generators are very reliable and tend to be comparatively inexpensive. Also mechanical properties, like generator slip causing the speed to slightly increase or decrease if the torque varies, makes it useful in for instance wind turbines.[19] In appendix A modelling of an asynchronous machine with a rotating two axes reference frame is presented.

It is the rotor that makes the asynchronous generator different from the synchronous generator. A squirrel cage rotor consists of a number of copper or aluminium bares which are connected electrically by aluminium end rings. The rotor is placed in the middle of the stator which is directly connected to the three phases of the electrical grid.

A squirrel cage asynchronous generator, also called induction generator, and a fixed capacitor forms the distributed generation in the case presented. The capacitor bank is implemented for magnetization of the asynchronous machine in order to have correct operation. The size of this capacitor bank is

found by adjustment in the simulation model to obtain nominal voltage on the generator terminals. 260 kVar is found to be a suitable size and corresponds well to the general relation of real power P, reactive power Q and apparent power S given in equation 3.8. The 750 kW nominal real power of the generator and 260 kVar reactive power from the capacitor bank gives an apparent power of 794 kVA. This is close to the chosen base power in equation 3.1. However this is not entirely accurate because some reactive power is drawn from the capacitive filter of the converter to the generator during steady state operation.

$$S^2 = P^2 + Q^2 \tag{3.8}$$

With these power values the power factor is given in equation 3.9. The angle is capacitive because current is leading voltage.

$$\begin{aligned} \cos\varphi = \frac{P}{S} = \frac{750kW}{794kVA} &= 0.94458 \\ \varphi = \arccos\frac{P}{S} &= -19.16\,\mathrm{deg} \end{aligned} \tag{3.9}$$

The asynchronous generator implemented in the simulation model has parameters as shown in table 3.1.

3.4 The Transformers

Two identical transformers are inserted in the distribution system under study. With these transformers the system has two voltage levels. The Y-Δ connection is shown in figure 3.2. This coupling produces a phase shift. Star point of the Y-winding is earthed. Y-winding is chosen as primary winding with a voltage level of 690 V while Δ-winding is secondary winding and operate at 22 kV. Assuming an ideal transformer core, and disregarding saturation and magnetizing current. Configuration of transformers are summed up in table 3.2.

3.5 Three-Phase Distribution Grid

The 22 kV distribution grid is modelled as a weak grid and represented by a three-phase voltage source behind a resistance and an inductance. Parame-

Parameters of asynchronous machine	
Nominal power	750000 $[W]$
Nominal voltage	690 $[V_{3ph,rms}]$
Nominal current	628 $[A_{rms}]$
Nominal frequency	50 $[Hz]$
Pole pairs	2
Stator resistance	0.0092 $[pu]$
First cage resistance	0.0076 $[pu]$
Second cage resistance	10 $[pu]$
Stator unsaturated leakage reactance	0.1580 $[pu]$
Unsaturated magnetizing reactance	3.8693 $[pu]$
Rotor unsaturated mutual reactance	0.0651 $[pu]$
Second cage unsaturated reactance	10 $[pu]$
Polar moment of inertia	10 $[s]$
Mechanical damping	0.008 $[pu]$

Table 3.1: Parameters for asynchronous machine implemented in simulation model

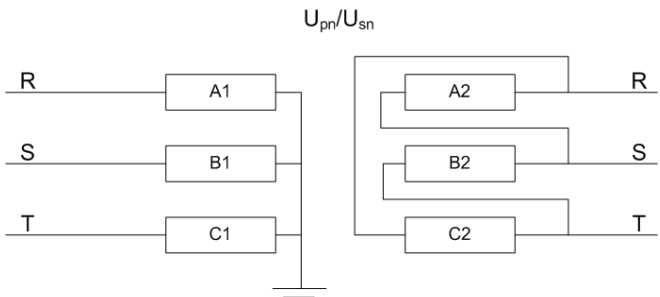

Figure 3.2: Y-Δ transformer coupling with earthed star point.

Configuration of transformers	
Nominal power	800000 $[VA]$
Nominal frequency	50 $[Hz]$
Winding 1 type	Y
Winding 1 nominal voltage	690 $[V_{3ph,rms}]$
Winding 2 type	Δ
Winding 2 nominal voltage	22000 $[V_{3ph,rms}]$
Delta lags or leads Y	Lags
Positive sequence leakage reactance	0.06 $[pu]$
Ideal transformer model	Yes
No load losses	0.001 $[pu]$
Copper losses	0.01 $[pu]$
Saturation enabled	No

Table 3.2: Configuration of transformers implemented in simulation model

ters are given in table 3.3.

Parameters of distribution grid	
Nominal voltage	22000 $[V_{3ph,rms}]$
Nominal frequency	50 $[Hz]$
Resistance	2 $[\Omega]$
Inductance	0.05 $[H]$

Table 3.3: Parameters of distribution grid implemented in simulation model

Lines

There are three lines included in the system as seen in figure 3.1. Resistances in the lines are neglected for the lines between distribution system and grid because the values are too small compared to reactances. The reactance Lp from distribution grid to load is much smaller, but resistance is neglected here also for simplicity reasons. Capacitances between lines and to earth are neglected. Choosing an inductance value of 1 mH/km the lines get values as seen in 3.10

$$\begin{aligned} L_1 &= 1[mH] \\ L_g &= 50[mH] \\ L_p &= 0.1[mH] \end{aligned} \tag{3.10}$$

3.6 The Constant Power Load

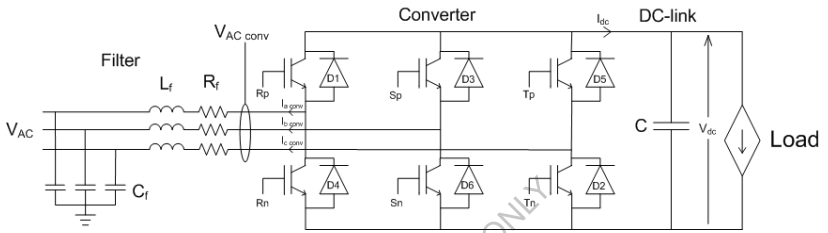

Figure 3.3: The implemented converter with load

Figure 3.3 display the CPL from converter filter to DC-link and load. L_f is chosen to be 5 % of base impedance. This is minimum required inductance for practical thyristor converters resolved by the German VDE standards[1]. Resistance R_f is chosen to be 1 % of base impedance. R_f and L_f are calculated in equation 3.11.

$$\begin{aligned} R_f &= 1\% \cdot Z_{b1} = 5.95[m\Omega] \\ L_f &= 5\% \cdot \frac{Z_{b1}}{2\pi f_n} = 0.0947[mH] \end{aligned} \tag{3.11}$$

A capacitive filter is inserted to filter out current sags and switching transients. C_f is chosen to have three capacitors of 1000 [μF].

The voltage source converter consists of IGBT switches with anti-parallel diodes that will conduct reverse current. Switching of these IGBTs is done by a pulse width modulation (PWM) technique at a frequency of 5 [kHz]. A DC-link capacitor with a value of 4000 [μF] is connected in parallel to the load. This load is modelled as a dependent current source that use a manually specified value of power divided by measured dc voltage. This is depict in figure 3.4

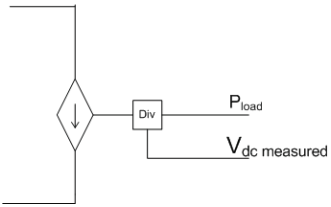

Figure 3.4: Configuration of load.

3.7 Control of converter

The converter control is the most essential area of the thesis and will be thorough explained.

A voltage oriented vector control is implemented to maintain the real power to the load constant. This control strategy is advantageous for its fast dynamics and decoupled control ability[20]. The control scheme of the converter with ability to control reactive current is shown in figure 3.5.

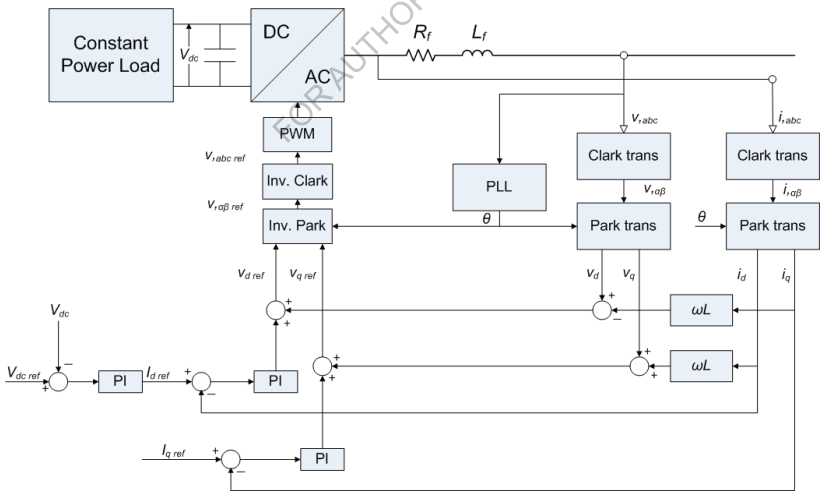

Figure 3.5: Converter control diagram when the converter has reactive current control

By keeping i_{qref} fixed at zero and excluding v_q and $i_d \cdot \omega \cdot L$ the converter

does not compensate reactive current during faults. The control scheme then looks like figure 3.6.

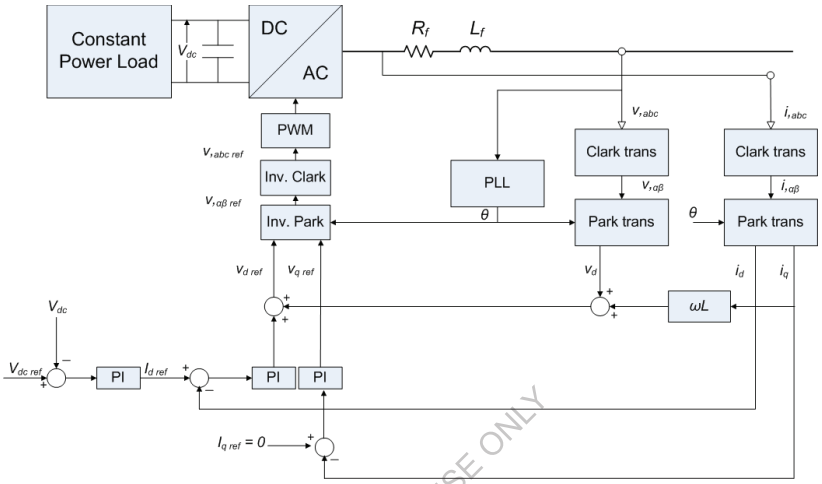

Figure 3.6: Converter control diagram when the converter does not have reactive current control

Each block in these schemes will be explained in the following subsections.

3.7.1 Two phase representation

With the chosen control strategy a two-axis system is desirable in contrast to the three-phase stationary axis system. The d-q rotating coordinate system simplifies the representation of voltage and current. The transformation is done through the α-β stationary coordinate system.

Clark transformation

Clark transformation convert the phase values of voltage and current into stationary α-β reference frame. Opposite will the Inverse-Clark transformation convert stationary α-β quantities to three-phase stationary quantities. The two coordinate systems are shown in figure 3.7.

α-axis is aligned with the three phase a-axis to keep the analysis as simple as possible. The matrix for clark transformation is shown below.

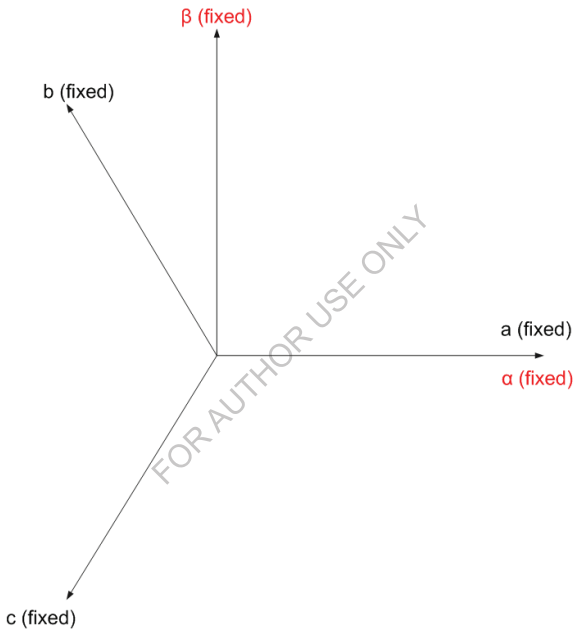

Figure 3.7: The three-phase coordinate system(black) and the α-β coordinate system(red)

$$\begin{bmatrix} v_\alpha \\ v_\beta \\ v_0 \end{bmatrix} = \frac{2}{3} \cdot \begin{bmatrix} 1 & -\frac{1}{2} & -\frac{1}{2} \\ 0 & \frac{\sqrt{3}}{2} & -\frac{\sqrt{3}}{2} \\ \frac{1}{2} & \frac{1}{2} & \frac{1}{2} \end{bmatrix} \cdot \begin{bmatrix} v_a \\ v_b \\ v_c \end{bmatrix} \tag{3.12}$$

Note that v_0 denotes a zero-sequence voltage, which is assumed to be zero. This voltage would only have non-zero values for unbalanced conditions. The presumption of symmetric currents and phase voltages that sum up to zero justifies to neglect the zero sequence[21]. With this assumption the matrix looks like equation 3.13. This matrix is used in the model built for this thesis and for the following calculations.

$$\begin{bmatrix} v_\alpha \\ v_\beta \end{bmatrix} = \frac{2}{3} \cdot \begin{bmatrix} 1 & -\frac{1}{2} & -\frac{1}{2} \\ 0 & \frac{\sqrt{3}}{2} & -\frac{\sqrt{3}}{2} \end{bmatrix} \cdot \begin{bmatrix} v_a \\ v_b \\ v_c \end{bmatrix} \tag{3.13}$$

The matrix for Inverse-Clark transformation is given in equation 3.14.

$$\begin{bmatrix} v_a \\ v_b \\ v_c \end{bmatrix} = \begin{bmatrix} 1 & 0 \\ -\frac{1}{2} & \frac{\sqrt{3}}{2} \\ -\frac{1}{2} & -\frac{\sqrt{3}}{2} \end{bmatrix} \cdot \begin{bmatrix} v_\alpha \\ v_\beta \end{bmatrix} \tag{3.14}$$

Park Transformation

Park transformation convert the stationary α-β reference frame into synchronously rotating d-q reference frame. The d-q reference frame is rotating at speed ω with respect to the stationary α-β reference frame. The position of d-axis is at any instant given by equation 3.15 with respect to α-axis. Opposite will the Inverse-Park transformation convert the rotating d-q coordinate system to the stationary α-β coordinate system. The three coordinate systems are shown in figure 3.8.

$$\theta = \omega \cdot t \tag{3.15}$$

The matrix showing the Park transformation is given in equation 3.16 and the Inverse-Park in equation 3.17.

$$\begin{bmatrix} v_d \\ v_q \end{bmatrix} = \begin{bmatrix} cos\theta & sin\theta \\ -sin\theta & cos\theta \end{bmatrix} \cdot \begin{bmatrix} v_\alpha \\ v_\beta \end{bmatrix} \tag{3.16}$$

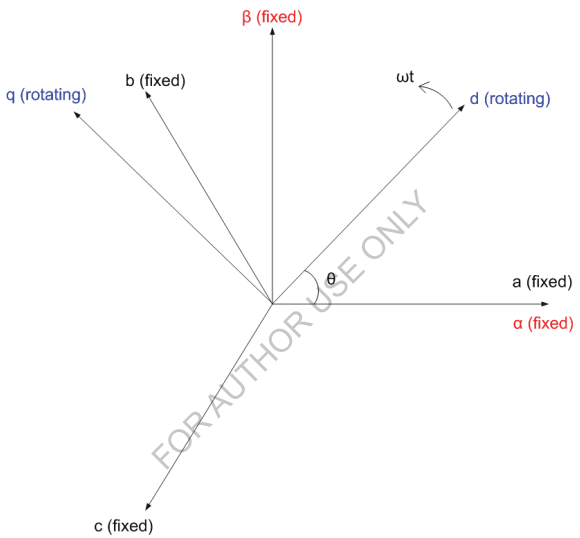

Figure 3.8: The three-phase stationary coordinate system(black), the α-β stationary coordinate system(red) and the rotating d-q coordinate system(blue). θ is the angle between α-axis and d-axis at any instant. ω is the angular speed of the d-axis with respect to α-axis.

$$\begin{bmatrix} v_\alpha \\ v_\beta \end{bmatrix} = \begin{bmatrix} cos\theta & -sin\theta \\ sin\theta & cos\theta \end{bmatrix} \cdot \begin{bmatrix} v_d \\ v_q \end{bmatrix} \tag{3.17}$$

Variables in both clark and park transformations are given as voltages, but the same matrices are used on current transformations.

3.7.2 Phase Locked Loop

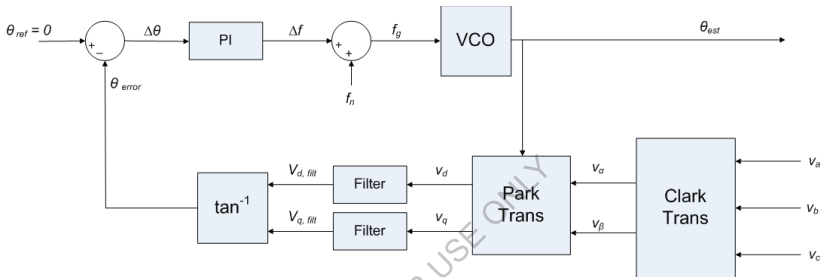

Figure 3.9: Structure of PLL

A Phase Locked Loop (PLL) is basically a closed loop frequency control system. Its function is to control the angle θ seen in figure 3.8.

By transforming measured phase voltage to a rotating dq-reference frame the PLL detects the phase of the grid voltage referred to the grid voltage space vector. A filter smooths the d- and q- components of the voltage to attenuate noise. An arc tan function calculates the phase of the voltage in all four quadrants.

The reference angle θ_{ref} is preferably set to zero and the deviation from this value is fed into a PI-regulator. The output of the PI-regulator is the deviation from the base frequency. By adding the base frequency the actual grid frequency is obtained. The grid frequency inputs a Voltage Controlled Oscillator (VCO) which in this case is an integrator that outputs a triangle waveform between 0 and 2π with a period corresponding to the grid frequency.

This output angle is used as an input to the dq-transform, closing the loop. It is also used in the inverse park transformation and park transformation of measured phase currents.

The PLL is in lock as long as the estimated angle output is correct. Then the input of the PI-regulator is constant and it outputs a constant value corresponding to the real frequency of the grid. If the angle differs from the grid angle(caused by for instance faults), the frequency is adjusted by the PI-regulator and the grid angle estimate is changed until the loop is in lock again.[21]

Comparison of the PLL output θ_{est} and the input phase voltage is shown in chapter 4.

3.7.3 DC-link voltage control

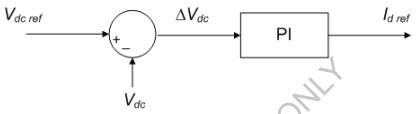

Figure 3.10: DC-link control block

The DC link voltage control is responsible for keeping the DC voltage constant at a specified value. In this case it is desirable to keep it at the value given in equation 3.4. This reference value is compared with the measured value and the difference is run through a PI regulator. The output is used as reference value for I_d in the current control. This control is visualized in figure 3.10.

3.7.4 Current control

The reference voltage for the PLL is V_{AC} in figure 3.3 and current reference for the control system is $I_{abcconv}$ in the same figure. Hence V_{AC} can be derived as:

$$V_{AC} = V_{ACconv} - R_f I_{abcconv} - L_f \frac{dI_{abcconv}}{dt} \tag{3.18}$$

where V_{AC} is voltage at the capacitive filter, V_{ACconv} and $I_{abcconv}$ is voltage and current at converter, R_f is resistance and L_f is filter inductance. Transforming equation 3.18 into dq- reference frame yield this equation:

$$\begin{bmatrix} v_d \\ v_q \end{bmatrix} = \begin{bmatrix} v_{dconv} \\ v_{qconv} \end{bmatrix} - R_f \begin{bmatrix} i_d \\ i_q \end{bmatrix} - L_f \frac{d}{dt} \begin{bmatrix} i_d \\ i_q \end{bmatrix} - L_f \begin{bmatrix} 0 & -\omega \\ \omega & 0 \end{bmatrix} \begin{bmatrix} i_d \\ i_q \end{bmatrix} \tag{3.19}$$

From equation 3.19 it is possible to derive equations for each of the current controllers:

$$v_{dconv} = v_d + R_f i_d + L_f \frac{di_d}{dt} - \omega L_f i_q \tag{3.20}$$

$$v_{qconv} = v_q + R_f i_q + L_f \frac{di_q}{dt} + \omega L_f i_d \tag{3.21}$$

These equations are found to control the current flowing through the CPL and define the voltage needed to achieve constant DC voltage. The q-axis current controller is used to control reactive power while the d-axis current controller controls the amount of active power. Current controllers are depict in figure 3.11. ω is grid frequency and the speed in which the dq- reference frame rotate with respect to stationary a- axis. In this thesis the d- axis voltage vector is aligned with the grid voltage vector and consequently q-axis voltage vector is 0.

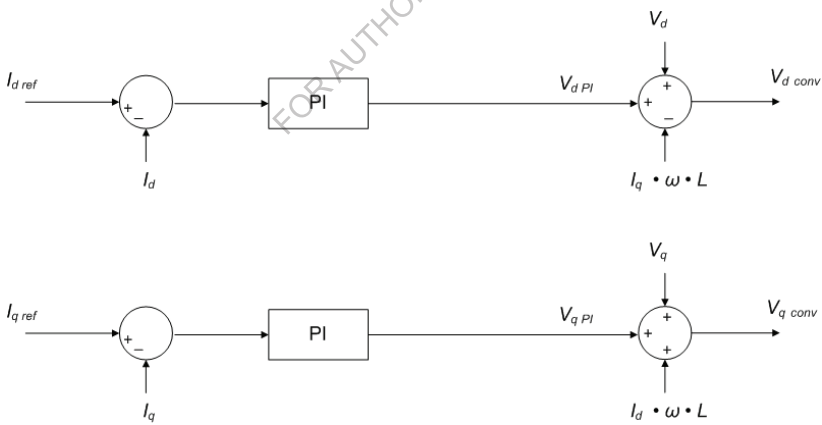

Figure 3.11: d-axis and q-axis current controllers respectively.

All values are per unit values referred to d- and q- axes. The q-axis current controller in figure 3.11 is for the case of reactive current control. For the case of no reactive control v_q and $\omega \cdot L_f \cdot i_d$ is cancelled out and i_{qref} is set to 0.

3.7.5 PWM

The Pulse-width-modulated (PWM) three-phase inverter shape and control the three-phase output voltage in magnitude and frequency with the constant input voltage V_{dc}. A triangular voltage waveform is compared with the three-phase reference voltage estimate from the inverse clark transformation. These voltages are 120 degrees out of phase and responsible for the IGBT switching.

Figure 3.12 shows the triangular voltage and each control phase voltage. V_d in the figure demonstrate the input DC voltage. When v_{AN} is equal to V_d one IGBT on a inverter leg is on and conducts current. When this IGBT switch off and v_{AN} is zero the other IGBT is switched on. Hence there will always be one switch on every leg conducting current.

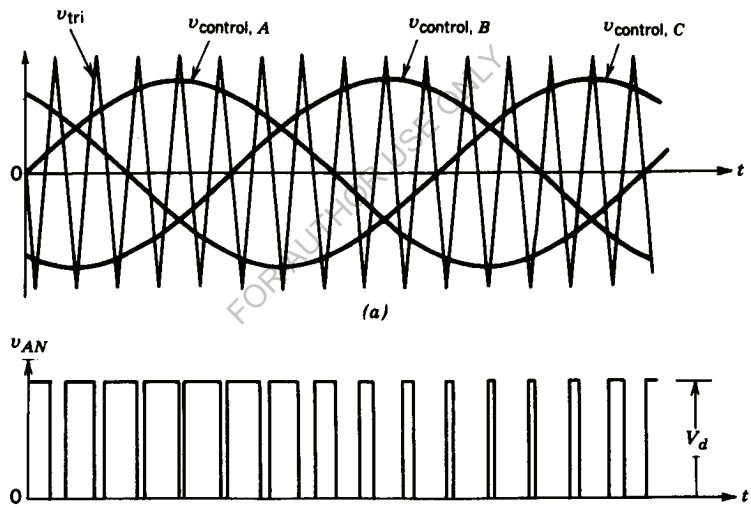

Figure 3.12: Three-phase PWM waveform. Depicts a triangular voltage signal, three control phase voltages and one output(referred to inverter) phase voltage v_{AN}[1].

Over-modulation is the area above linear modulation in figure 3.13. What happens is that the peak of the control voltage is allowed to exceed the peak of the triangular waveform. As a consequence the switches will be on or off at the period in which the reference voltage is above or beneath the triangular voltage signal. This causes great instabilities in the converter control and

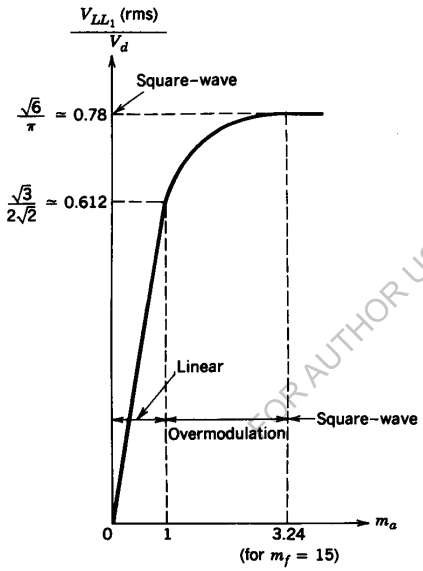

Figure 3.13: Linear and over-modulation ranges for a three-phase inverter[1].

the AC system. m_a in figure 3.13 is the amplitude modulation ratio. In equation 3.4 m_a is set to be 1 and kept within the linear region ($m_a \leq 1$).

3.8 Measurement

Distributed generation

Measurements of mechanical and electrical torque, output speed, and real and reactive internal machine power are taken from "internal output variables" in the induction machine implemented in the model. Phase voltages and currents, and real and reactive power from the distribution system are measured on the lines between the capacitor bank and the transformer.

CPL

Real and reactive power are measured both over L_f in figure 3.3 and at the point of common coupling to see how much power flows through the load and how much reactive power is generated by the capacitive filter and by reactive current injection. Current is measured in front of the converter before it is filtered and voltage measurement is done at the terminal of the capacitive filter. These voltages and currents are used as input to the converter control. Another input to the converter control is the DC-link voltage measured between capacitor and load.

Grid

Power measurement is done across L_g to measure the amount of power that is transported to the grid, or delivered from the grid.

Results

Voltages and currents are measured at the output of the two park transformations.

Chapter 4

Simulations With A Constant Power Load

4.1 System description

The simulation model is built in PSCAD/EMTDC simulation software. It is made with the simulations master students Moltoni and Fascendini have done in MATLAB SIMULINK[10] as background. Some adjustments have been done to make the model run smoother. This includes reducing the line between load and grid. This chapter explains the system from generator to grid, including control system of converter, through simulation. Simulation blocks are reported in appendix B.

In the first case the system is run without any faults or other interference reaching steady state. The objective is to explore the system from generation to grid.

4.1.1 Operation of the distributed generation

The squirrel cage induction machine can be operated in either speed control or torque control modes. To start up the machine it is run at 1.005 p.u. with respect to nominal speed. After the initial transients of the machine die out, at about 1 second, the machine is switched to torque control with a specified value of -1 p.u. The minus indicates that the machine operates as a generator. As seen in figure 4.2 the mechanical torque has a instantaneous step while the electrical torque reach a steady state value of -0.992 p.u. after a step response lasting 1.5 seconds. In the same time period the rotor speed increase from 1.005 to 1.0085 p.u.

The internal generator powers are plotted in figure 4.3. Power direction is referred into the machine, hence the real power is negative(produce power)

and reactive power is positive(absorb power). The powers are given in per unit values of the nominal machine parameters given in table 3.1. Steady state value of real power is measured to 0.98 p.u. giving a value of 735 kW produced. Absorbed reactive power by the generator during steady state is 0.49 p.u. corresponding to 369 kVar.The generator absorb about 107.5 kVar from the capacitive converter filter.

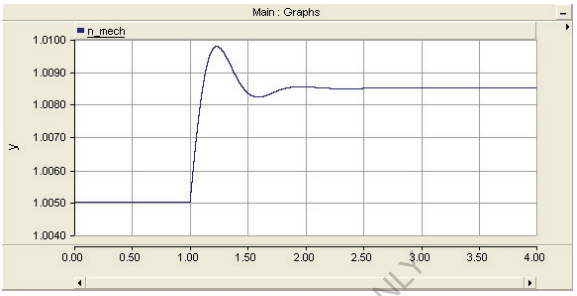

Figure 4.1: Rotor speed

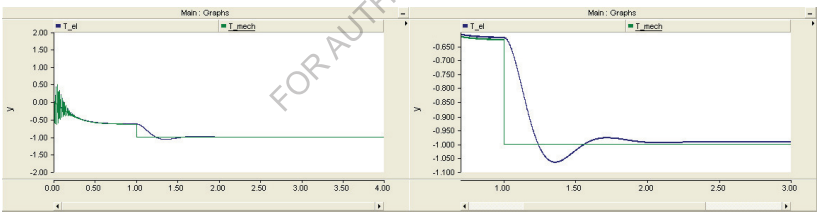

(a) Torque (b) Corresponding zoom

Figure 4.2: Electromagnetic torque(blue) and mechanical torque(green)

4.1.2 Voltages

After an initial transient the voltage at the generation terminals reaches base value, or 1 per unit. This voltage is reached by regulation of the fixed capacitor. As it is possible to observe in figure 4.4b and figure 4.5b the voltage at generation and load has a sinusoidal trend. Load voltage is measured at PCC between load transformer and grid.

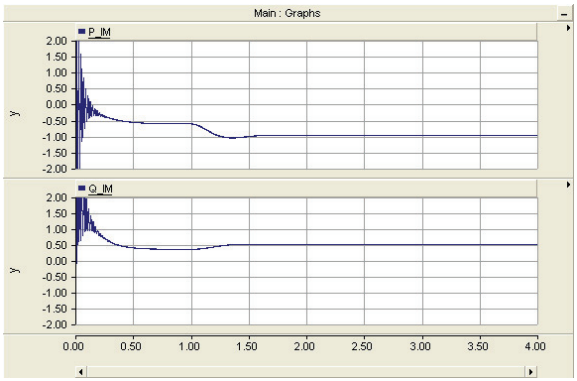

Figure 4.3: Internal real and reactive power of the asynchronous generator.

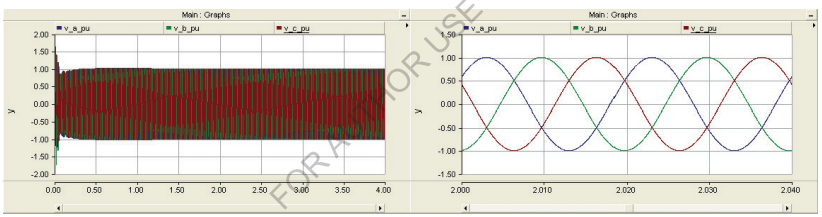

(a) Voltage (b) Phase voltages

Figure 4.4: Generation voltage

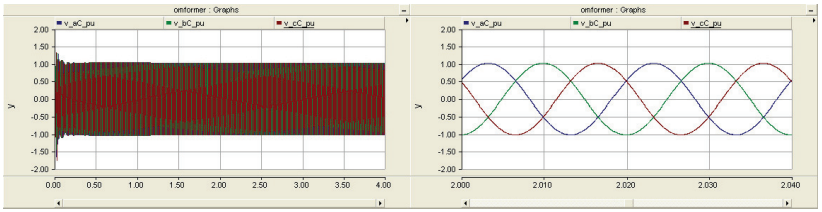

(a) Voltage (b) Phase voltages

Figure 4.5: Load voltage

4.1.3 Introducing Constant Power Load

Now focus is set to the effect of the load on this system. After two seconds the load is set to draw 220 kW, which is about 30 % of the generated real power. The flow of power in the system is displayed in figure 4.6. Power from the distribution system, termed P_{gen} and Q_{gen}, if fairly unaffected while about 30 % of the active grid power is taken by the load. The directions of power measurement are from generator to load, from load to PCC and from PCC to grid respectively. The amount of reactive power remains relatively constant.

After verifying the effect of the load on system power the next step is to look into the load itself.

DC-link

The DC-link voltage shown in figure 4.7 has a transient lasting 80 ms with a peak of 1.16 p.u. before stabilizing at 1 p.u. Note that the voltage has a small drop when the load switches on. Keeping this voltage stable at the specified value is important in regard to control system and load.

The PWM current is the blue graph in figure 4.8 and the green graph is the load current. The capacitor in parallel with the load functions as a current filter for the load and absorbs the current transients.

4.1.4 The Control System

PLL

Measured voltage at the capacitive filter is run through clark and park transformation and used as input to the PLL. The resulting d- axis and q- axis voltage is shown in figure 4.9. Note that the q- axis voltage is zero because the d- axis component is aligned with the grid voltage vector. The PLL then measure the frequency of the three phase voltage and calculate the angle θ. Comparing the phase voltage with θ in figure 4.9 it can be concluded that they have the same period time.

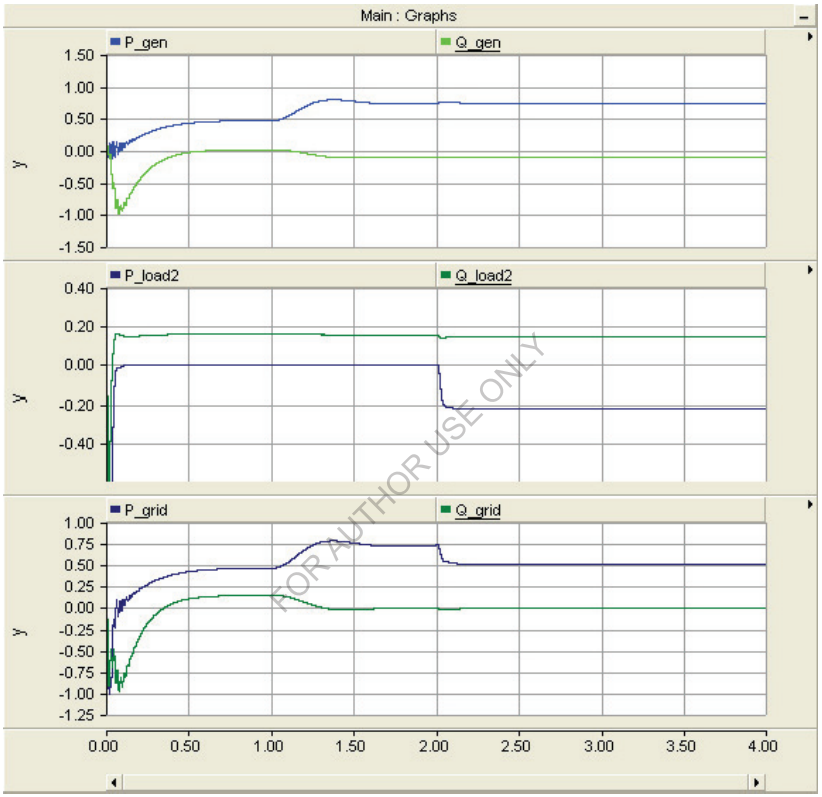

Figure 4.6: Real and active power throughout the system with the load switching on after 2 seconds. P_{gen} and Q_{gen} are power from the distributed generation, P_{load2} and Q_{load2} are power from the load at PCC, and P_{grid} and Q_{grid} are power flowing to the grid. The reactive power from the load is generated in the capacitive filter of the converter.

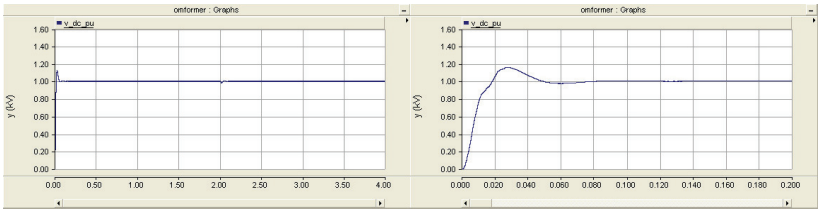

(a) DC voltage (b) Start sequence of DC voltage

Figure 4.7: DC-link voltage

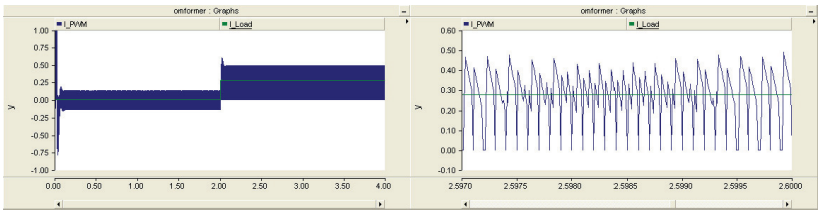

(a) DC current (b) Zoomed DC current

Figure 4.8: Current on the DC side of the converter. I_{PWM} is the unfiltered current coming from the converter and I_{Load} is the load current computed from the real power output divided by measured DC voltage.

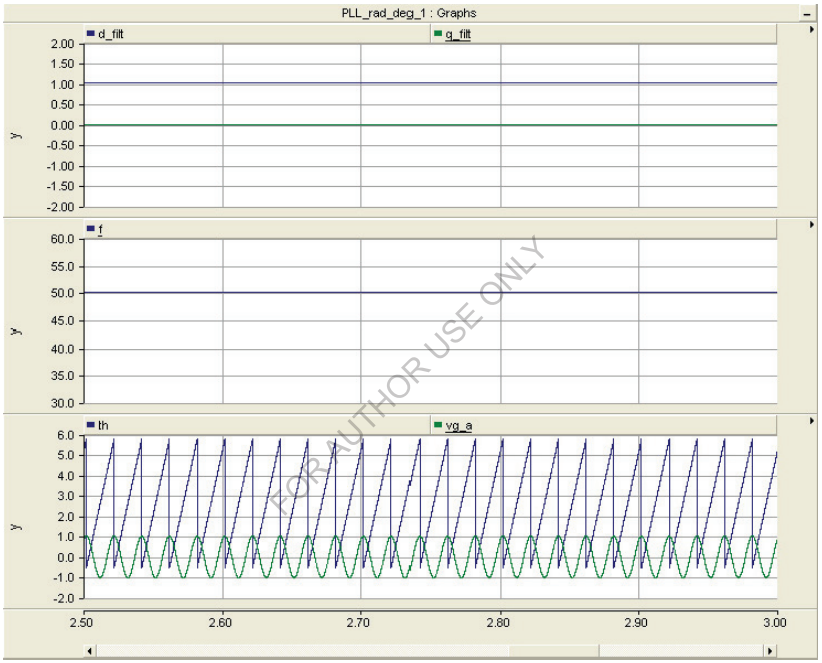

Figure 4.9: d_{filt} and q_{filt} are voltages in the rotating two axes reference frame. f is the measured grid frequency. θ is the resulting angle used in the park and inverse park transformation.

Current control

The measured current is run through clark and park transformation as for the voltage. After the transformation into rotating current vectors these currents are subtracted from the reference values in the current control block. The currents are shown in figure 4.10. From the figure it can be concluded that it is only the d- component of the current that is affected by the load. The q-component is kept at zero and no reactive current is injected.

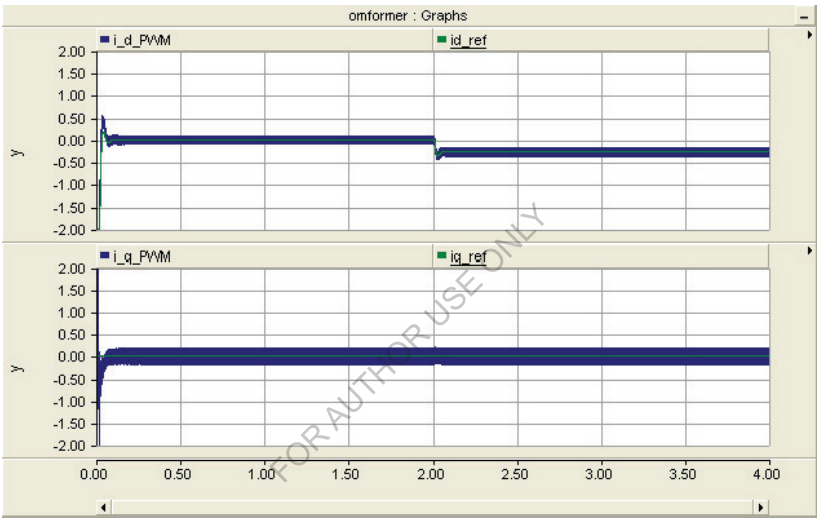

Figure 4.10: i_{dPWM} and i_{qPWM} are measured currents referred to the rotating two axes reference frame. i_{dref} and i_{qref} are the reference currents from the DC-link voltage control and the manually controlled reactive current.

Resulting voltage from the current controllers are then transformed back into three phase control voltages for the PWM through inverse park and inverse clark transformations. This sequence is shown in figure 4.11. The three phase control voltages are injected with a third harmonic signal to avoid over-modulation in the PWM.

PWM

Pulse-width-modulation is the last step of the converter control. Figure 4.12 shows the triangular voltage signal and one control phase voltage. The graph

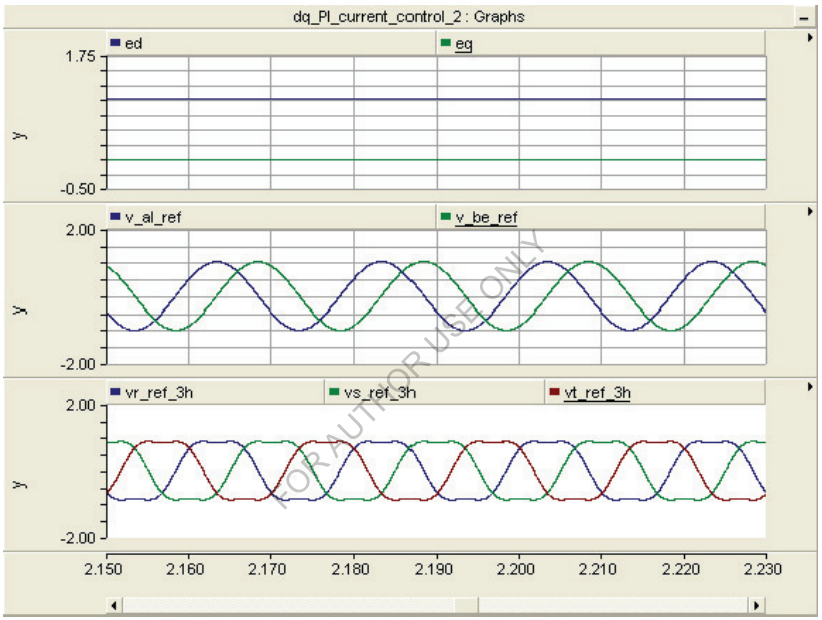

Figure 4.11: This figure shows the inverse park and inverse clark transformation from the output current control voltage to the PWM control voltage. *ed* and *eq* refer to dq- voltages,v_{alref} and v_{beref} refer to $\alpha\beta$- voltages, and v_{rref3h}, v_{sref3h} and v_{rref3h} refer to abc- voltages.

beneath shows how one IGBT is switched on and off as the control voltage is over or below the triangular voltage signal.

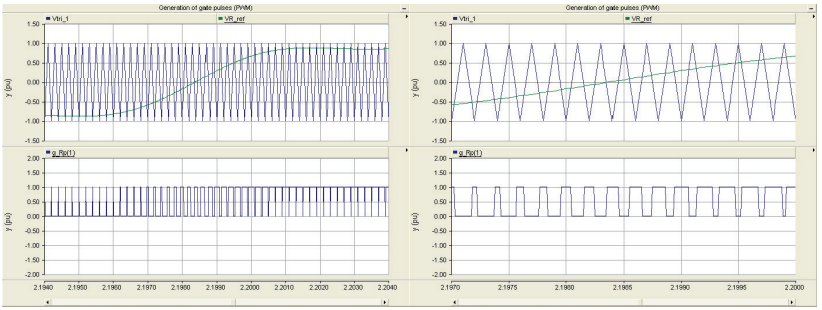

(a) PWM (b) More zoomed PWM

Figure 4.12: PWM switching scheme with one control voltage and the switching of one IGBT.

As a verification of the theory explained with regard to over-modulation the DC-link voltage is lowered to 0.85 p.u. and the concept of over-modulation becomes visual. The control voltage peak increase beyond the triangular voltage signal and the converter control does not work properly. Open or closed switches at long periods of time result in instability in the whole converter due to loss of control with current and voltage. The case of over-modulation is shown in figure 4.13.

4.2 Simulations to verify constant power load

Since one of the tasks of this work is to make a simulation model with a constant power load it is desirable to verify that the load behave as a CPL. Obtaining the negative resistance curve in figure 2.5 will satisfy the aim. This can be achieved by implementing a three phase resistive fault in the grid between load connection and L_g. The fault resistances are regulated to obtain voltage drops in the system. The resistive fault is designed as in figure 4.14. In these simulations the control scheme in figure 3.6 is used.

Measurement of d-component of voltage(remember that the q-component is zero) and d-component of current are done for every voltage drop. These values are taken from the control system. Output rotating two phase voltage

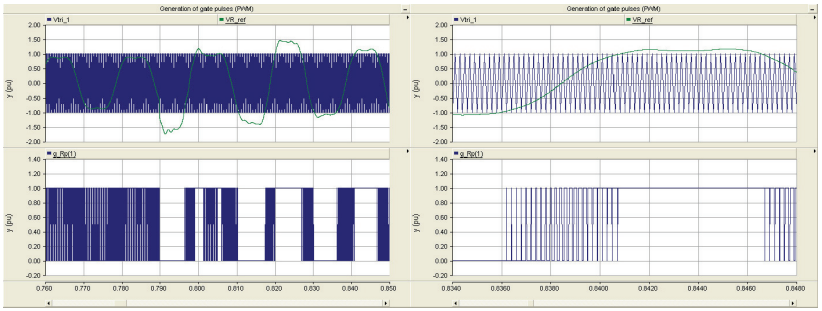

(a) Over-modulation (b) Zoomed over-modulation

Figure 4.13: The PWM goes into over-modulation mode as a consequence of decreased DC-link voltage. The IGBT is only switching when the control voltage is within the triangular voltage signal.

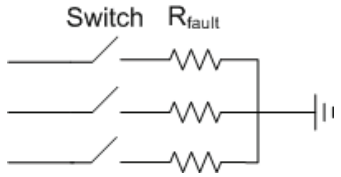

Figure 4.14: The three phase to ground fault placed beside load at grid.

from the PLL and input current to the current controllers are used in this experiment.

In these simulations the load is still drawing 220 kW, but now it is active from the start of the simulation. The fault is set to switch on 2 seconds into simulation and last 0.5 seconds.

The aim is to find fault resistances which result in 0.1 p.u. voltage drop between each measurement. Steady state value for the voltage is found to be 1.019 p.u. and 0.272 for the current. After some trail and error 64 Ω where found to get a voltage of 0.9 p.u. With this voltage the current is 0.307 p.u. This can be seen in figure 4.15 and figure 4.16.

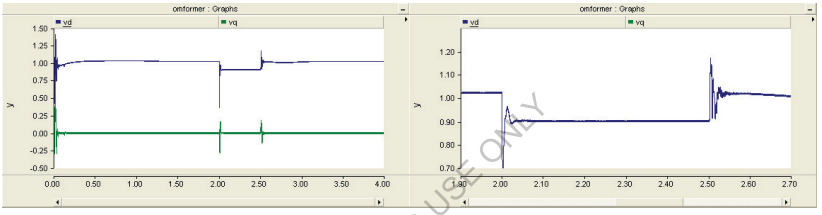

(a) Phase voltages (b) Zoomed d-axis voltage at fault

Figure 4.15: Voltages with a fault emerging at 2 seconds and lasting 0.5 seconds. The d-axis voltage drops to 0.9 p.u. while the q- axis component remains at zero during the fault.

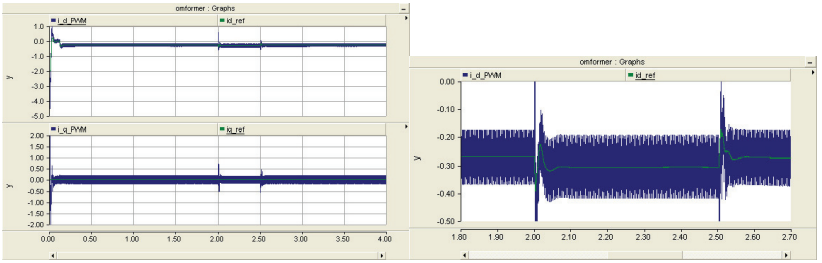

(a) Phase currents (b) Zoomed d-axis current at fault

Figure 4.16: Currents with a fault emerging at 2 seconds and lasting 0.5 seconds. The d-axis current increase from 0.272 p.u. to 0.307 p.u. while the q- axis component remains at zero during the fault.

The real and reactive power, measured over the inductive converter filter L_f, is depict in figure 4.17. The load draws constant real power and the reactive

power is zero during the fault. Direction of power measurement is set from grid to load in this case.

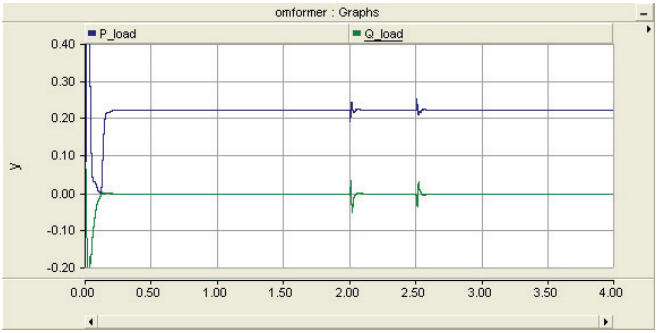

Figure 4.17: Real and reactive power at ac side of converter with a fault emerging at 2 seconds and lasting 0.5 seconds.

Results from these simulations are summed up in the result chapter.

4.3 Reactive current injection

Now focus is switched over to the effect of reactive current compensation on the ac voltage. The aim is to inject reactive current from the load to the grid to increase voltage and consequently make the system less vulnerable to instabilities. In these simulations the reactive current is injected throughout the whole simulation. As a consequence the voltage is increased also when there are no faults or other instabilities. For comparison the same values of fault resistance are used in these simulations as for the case with verification of CPL. The control scheme in figure 3.5 is used in these simulations.

The resistance is now set to 42.1 Ω which gave a voltage of 0.8 when there was no reactive current injection. In this case 0.2 p.u. reactive current is injected from the load. This result in the voltage seen in figure 4.18. The first thing to notice is that the steady state voltage is increased from 1.019 to 1.054. Secondly the voltage during the fault is increased from 0.8 to 0.83 p.u.

From the d-axis current component comparison in figure 4.19 it can be seen that the current is decreased from 0.272 to 0.263 in steady state and 0.347

to 0.335 in the case of a voltage drop of about 0.2 p.u. The q-axis current components in the two cases are shown in figure 4.20

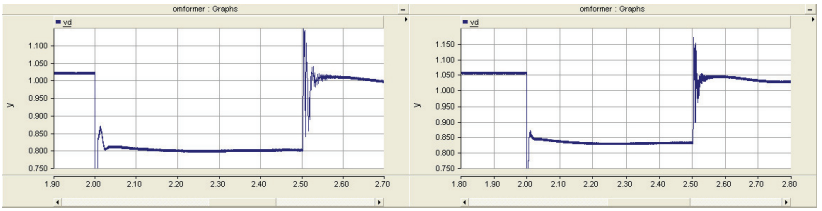

(a) Voltage without reactive current injection (b) Voltage with reactive current injection

Figure 4.18: Comparison of voltage with and without reactive current injection

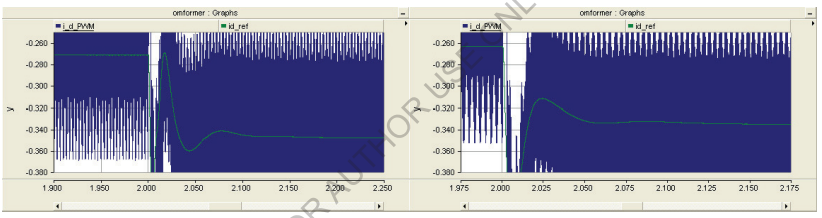

(a) d-axis current without i_q- injection (b) d-axis current with i_q- injection

Figure 4.19: Comparison of d-axis current with and without reactive current injection

The real power drawn by the load remains constant at the level manually imposed whilst the reactive power is a result of the d-axis voltage component and the amount of injected reactive current. The power relation is given by equation 4.1 and 4.2.

$$P = \frac{3}{2} \cdot (V_d \cdot I_d + V_q \cdot I_q) = CONST \tag{4.1}$$

$$Q = \frac{3}{2} \cdot (V_d \cdot I_q + V_q \cdot I_d) \tag{4.2}$$

As explained earlier V_q is zero because the d-axis is aligned with the grid voltage vector. This simplifies these expressions to:

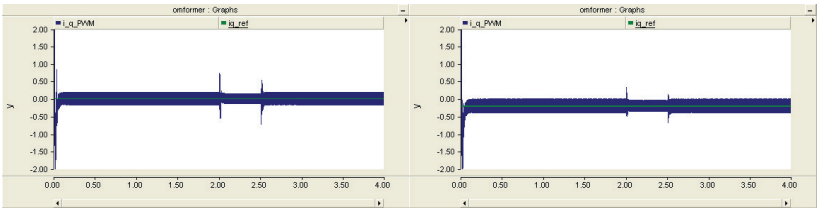

(a) q-axis current at zero (b) q-axis current at 0.2 p.u.

Figure 4.20: q-axis current in the two cases

$$P = \frac{3}{2} \cdot (V_d \cdot I_d) = CONST \tag{4.3}$$

$$Q = \frac{3}{2} \cdot (V_d \cdot I_q) \tag{4.4}$$

In figure 4.17 there is no I_q, hence there is no reactive power from the converter. With 0.2 p.u. reactive current injection the power relation becomes as in figure 4.21. The reactive power has a drop in power during the fault because it is proportional to V_d as seen in equation 4.4 while the active power is kept constant. It is fair to say that the load behaves as a CPL. The negative value of reactive power in figure 4.21 indicate that the reactive power is generated by the load, in contrast to the active power flowing into the load.

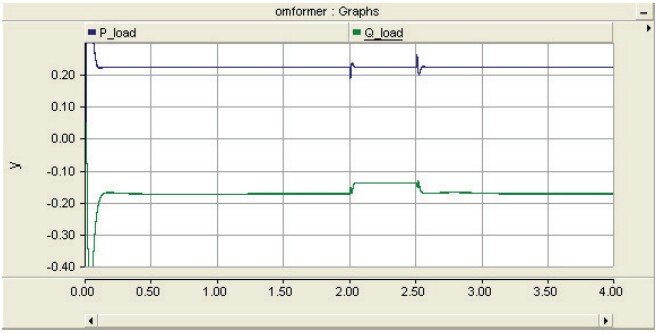

Figure 4.21: Real and reactive power at ac side of converter with 0.2 p.u. reactive current injection.

The simulation results from these simulations and simulations run with $I_q = 0.4$ p.u. are summed up in the result chapter.

Chapter 5

Simulation Results

5.1 Verification of negative resistance curve

As the aim of this thesis is to make a simulation model with a CPL it is desirable to verify that the CPL has negative resistance behaviour and in fact work as a CPL. This is done by measuring the d- component of voltage and current at the ac side of the converter at different faults. Decreasing fault resistance makes the voltage at the load decrease while the current increase. The curve in figure 5.1 demonstrate the behaviour of the CPL.

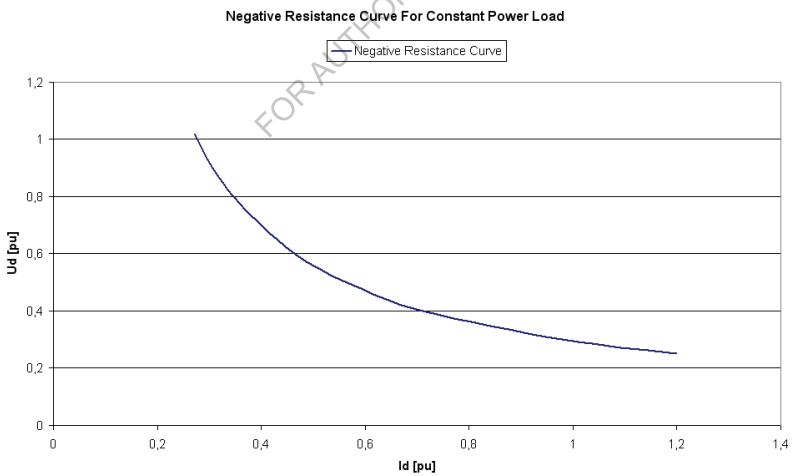

Figure 5.1: Negative resistance behavior of the CPL under study

Table 5.1 shows the values of the fault resistances used in the simulations and measured voltage and current.

Simulation results		
$Resistance[ohm]$	$V_d[pu]$	$I_d[pu]$
steady state	1.019	0.272
64	0.9	0.307
42.1	0.8	0.347
31.1	0.7	0.399
24.2	0.6	0.465
18.8	0.5	0.565
14.7	0.4	0.712
11.4	0.3	0.979
10.5	0.25	1.2
10.4	BD	BD

Table 5.1: Voltage and current with different fault resistances. With a fault resistance of 10.4 Ω the DC voltage collapse and the converter breaks down. Note that the resistance values are not related to the negative input resistance derived in equation 2.2.

5.2 Negative resistance curve with reactive current compensation

To investigate the effect of reactive current compensation simulations with current injection of $i_q = 0.2\,[pu]$ and $i_q = 0.4\,[pu]$ are done. The results are given in table 5.2 and visualized in figure 5.2.

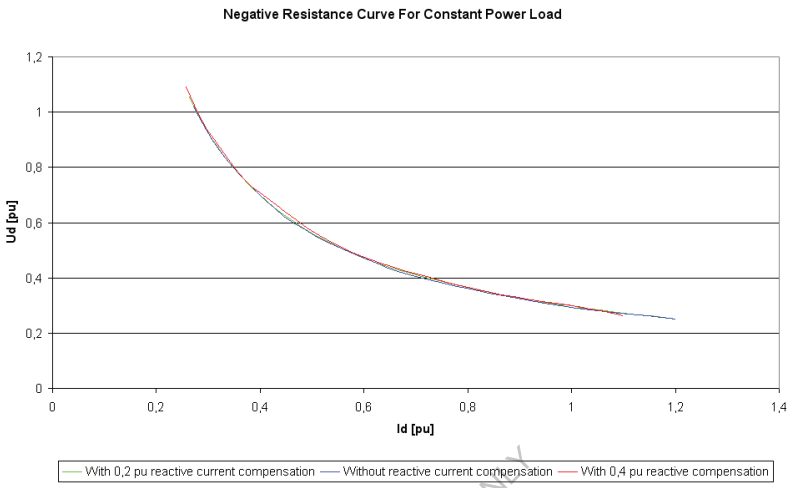

Figure 5.2: Negative resistance behavior of the CPL under study with(red and green curve) and without reactive current injection(blue curve).

Simulation results						
	$i_q = 0$		$i_q = 0.2$		$i_q = 0.4$	
$Resistance[ohm]$	$V_d[pu]$	$I_d[pu]$	$V_d[pu]$	$I_d[pu]$	$V_d[pu]$	$I_d[pu]$
steady state	1.019	0.272	1.054	0.263	1.09	0.257
64	0.9	0.307	0.933	0.298	0.965	0.29
42.1	0.8	0.347	0.83	0.335	0.86	0.326
31.1	0.7	0.399	0.726	0.384	0.754	0.372
24.2	0.6	0.465	0.629	0.446	0.665	0.43
18.8	0.5	0.565	0.526	0.536	0.552	0.514
14.7	0.4	0.712	0.428	0.666	0.453	0.632
11.4	0.3	0.979	0.328	0.888	0.356	0.82
10.5	0.25	1.2	0.295	1.01	0.324	0.912
10.4	BD	BD	0.291	1.02	0.320	0.924
9.8			0.250	1.20	0.296	1.01
9.7			BD	BD	0.292	1.02
9.3					0.263	1.1
9.2					BD	BD

Table 5.2: Voltage and current with different fault resistances. BD signify breakdown of the converter.

Chapter 6

Discussion

The results presented are measured on the ac side of the converter before the line between load and grid. Hence the effect of the load on the grid is not investigated to full potential. The measurements should have been done at the point where load connects to grid to see how the load influences the system voltage. However these results give a plain indication on the effect of reactive compensation.

The reactive current injection has been introduced to support the load voltage in case of a contingency. But with this control the current is injected also when there are no contingencies. This is not desirable because the reactive current does not contribute to the transfer of active power. Thus it only implies an increasing of the losses due to higher total current. The total current is I_T in figure 6.1. I_d is the active current and I_q is the reactive current. The appurtenant mathematical relation is given by equation 6.1.

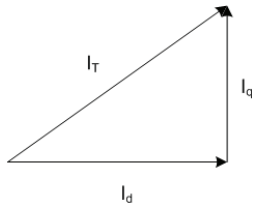

Figure 6.1: Current triangle showing the global current I_T, the active current I_d and the reactive current I_q.

$$I_T = \sqrt{I_d^2 + I_q^2} \tag{6.1}$$

Another drawback is the fact that this will be economically inconvenient for the users of the load because they have to pay for the generation of reactive power both when there is a contingency and during normal operation. A

control system that only generates reactive power during contingencies would make it more justifiable.

As the total current increase with increasing reactive current injection it is also important to increase the rating of the switches. The switches have to be rated according to the total current.

Only the active current I_d contribute to the flow of active power and the reactive current reduce the active current carrying capability. On the other hand it is positive in the sense that it support the voltage during voltage drops. As seen from the system it can handle greater fault before the converter breaks down.

Table 5.2 gives a better explanation of the principle of reactive current injection than figure 5.2. The changes in d-component voltage and current are not large enough to get a marked difference between the graphs. The steady state voltage value of 1.09 p.u. in the case of 0.4 p.u. reactive current injection is at the limit of what is acceptable pursuant to regulations in EN 50160. This state that slow variations of voltage having an amplitude until $\pm$ 10% of nominal value is acceptable.

Chapter 7

Conclusion

A simulation model has been built in PSCAD/EMTDC of a small distribution system. A description of the system trough theory and simulation has been presented. The constant power load in this system has been the main focus. Simulations with different voltage drops have been done to verify the CPL. By measuring the d-axis component of voltage and current for each voltage drop the resulting negative resistance curve could be delineated.

Simulations with and without reactive current injection have been compared with respect to voltage support. This shows that an injection of reactive current result in an increase of voltage both during steady state conditions and faults. An increase of reactive current results in increased voltage and a more rugged system in case of faults or other instabilities. With the reactive current injection a reactive power is transported from the load to the grid. This current does not contribute to the transport of active power but increase the losses and rating of the IGBT switches.

There are plenty of possibilities for further work. Improving the control system to only compensate reactive power when faults occur would remove some of the drawbacks of the control system. One way to solve this could be to use a voltage controller on the ac side of the converter to inject reactive current during voltage drops and to set boundaries on the amount of current injected in steady state.

It would also be interesting to upgrade the system to consist of more than one CPL and compare the reactive compensation with for instance a STATCOM. Case studies on which configuration gives the best voltage support and stability in the system could be done. Also upgrading the system to contain different kind of loads, like constant current loads, constant impedance loads or/and motor loads would be interesting. Generally investigate how the CPL work with different kinds of loads.

A more thorough investigation on transient stability effect with regard to

transient stability limit is desirable.

Bibliography

[1] Ned Mohan, Tore M. Undeland, and William P. Robbins. *Power Electronics - Converters, Applications and Design*. Wiley, 2003.

[2] The United Nations Framework Convention on Climate Change. `http://www.unfccc.int/`,24.6.2008.

[3] Innovasjon Norge, ENOVA, NVE, and Forskningsrådet. Fornybar energi 2007. Information paper, 2007.

[4] ECPE European Center for Power Electronics , EPE European power Electronics and Drives Association. Position paper on energy efficiency - the role of power electronics. In *European Workshop on Energy Efficiency-the Role of Power Electronics*, February 2007.

[5] Bimal K.Bose. Energy, environment, and advances in power electronics. *Proceedings of the 2000 IEEE International Symposium on Industrial Electronics*, 1:TU1–TU14, December 2000.

[6] N. Jenkins. Power electronics applied to the distribution system. *IEE Colloquium Flexible AC Transmission Systems - the FACTS*, pages 3/1–3/7, November 1998.

[7] Statnett. `http://www.statnett.no`,18.5.2008.

[8] NVE. `http://www.nve.no`,18.5.2008.

[9] A. Emadi, M. Barnes, N. Jenkins, and J.B. Ekanayake. Power quality and stability improvement of a wind farm using STATCOM supported with hybrid battery energy storage. *IEE Proceedings - Generation, Transmission and Distribution*, 153(6):701–710, November 2006.

[10] Duilio Moltoni and Gabriele Fascendini. Voltage support in ac distribution systems by power electronic loads. Master's thesis, Politecnico Di Milano, 2007.

[11] Wojciech A. Tobisz, Milan M. Jovanovic, and Fred C. Lee. Present and future of distributed power systems. *Proc. of the seventh annual applied power electronics conference and exposition APEC*, pages 11–18, February 1992.

[12] Ali Emadi. Modeling of power electronic loads in ac distribution systems using the generalized state-space averaging method. *IEEE Transactions on Industrial Electronics*, 51(5):992–1000, October 2004.

[13] N. Mithulananthan, M.M.A. Salama, C.A. Canizares, and J. Reeve. Distribution system voltage regulation and var compensation for different static load models. *International Journal of Electrical Engineering Education*, 37(4):384–395, October 2000.

[14] Mohamed Belkhayat, Roger Cooley, and Arthur Witulski. Large signal stability criteria for distributed systems with constant power loads. *Proc. of the IEEE Power Electronics Specialists Conference PESC*, 2:1333–1338, Jun 1995.

[15] Awang bin Jusoh. The instability effect of constant power loads. *Proc. of the National Power & Energy Conference, Kuala Lumpur, Malaysia*, pages 175–179, November 2004.

[16] Juan Dixon, Luis Morán, José Rodríguez, and Ricardo Domke. Reactive power compensation technologies: State-of-the-art review. *Proc. of the IEEE*, 93(12):2144–2162, December 2005.

[17] Ned Mohan. *Electric Drives - an integrative approach*. MNPERE, 2003.

[18] Ned Mohan. *Advanced Electric Drives - Analysis, Control and Modeling using Simulink*. MNPERE, 2001.

[19] Danish Wind Industry Association. `http://www.windpower.org`,19.6.2008.

[20] Marta Molinas, Jon Are Suul, and Tore Undeland. Improved grid interface of induction generators for renewable energy by use of STATCOM. *Proc. of the International Conference on Clean Electrical Power ICCEP, Capri, Italy*, pages 215–222, May 2007.

[21] Jon Are Wold Suul. Control of variable speed pumped storage hydro power plant for increased utilization of wind energy in an isolated grid. Master's thesis, Norwegian University Of Science And Technology, 2006.